Coloquio Nobel 2010

Liliana Arrachea
Departamento de Física
Universidad de Buenos Aires

Fabricando un gas bidimensional de electrones ''relativistas'' con lápiz y cinta Scotch

Premio Nobel de Física 2010

Konstantin Novoselov

André Geim

''por sus novedosos experimentos en el material bidimensional *grafeno*''.

Konstantín Serguéievich Novosiolov

(Константи□н Серге□евич Новосёлов)

- 23.08.1974, NizhnyTagil,URSS.
- Nacionalidad: Ruso-británico.
- Carrera de grado: Instituto de Física y Tecnología de Moscú.
- Doctorado:Radboud University Nijmegen, Holanda.
- Actualmente: Profesor de la Universidad de Manchester, Reino Unido.

Andre Konstantinovich Geim
(Андрей Константинович Гейм)

- 01.10.1958, URSS.
- Nacionalidad: Ruso, holandés, británico.
- Carrera de grado:Instituto de Física y Tecnología de Moscú.
- Doctorado: Instituto de Física del Estado Sólido de la Academia de Ciencias de Rusia.
- Postdoctorado: Nottinghan, Bath Copenhagen.
- 1994: Profesor de Radboud University Nijmegen, Holanda.
- 2001: Profesor de la Universidad de Manchester.

Grafeno

Estructura bidimensional de carbono de un átomo de espesor

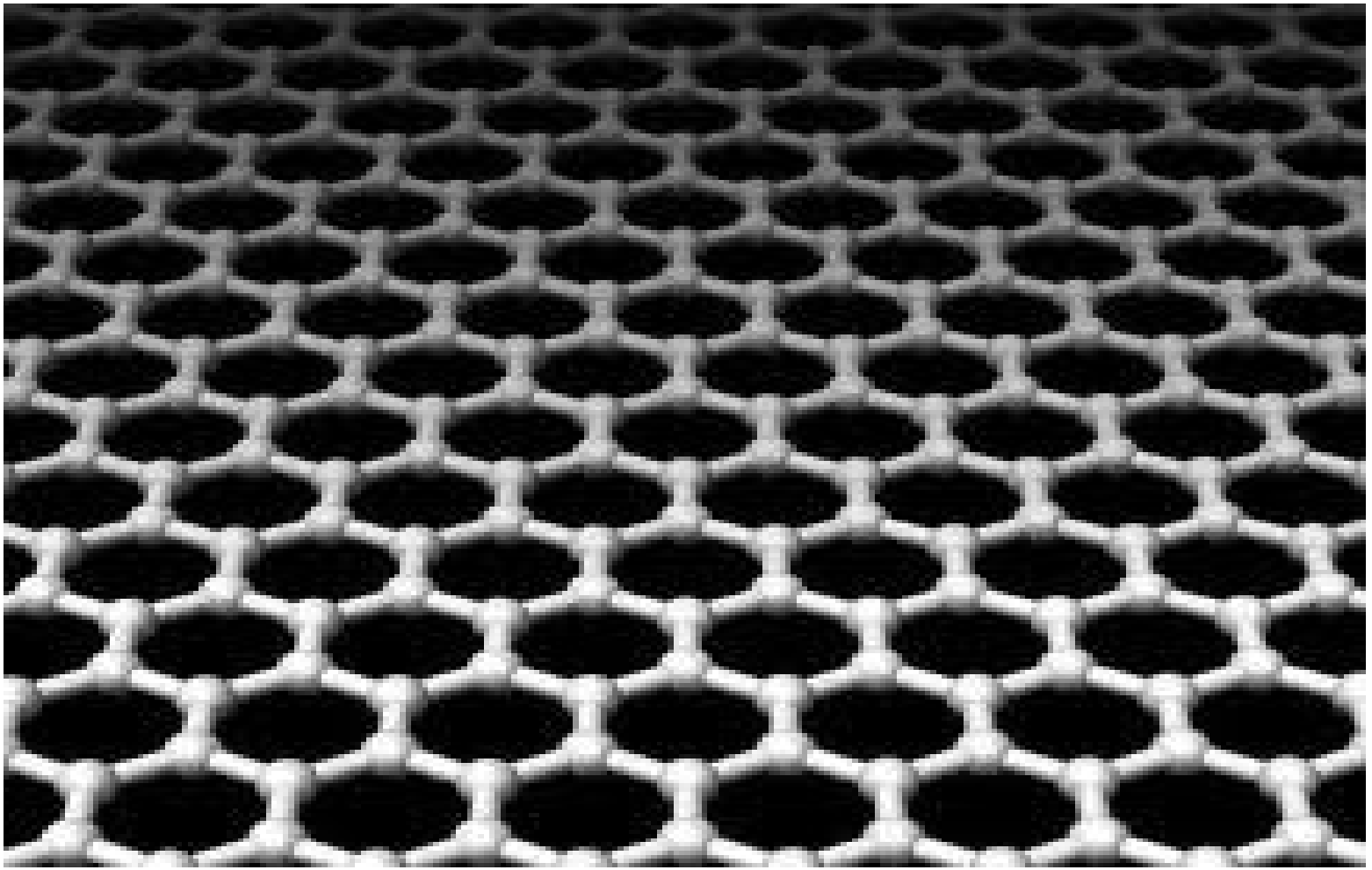

Otras formas del Carbono

3D

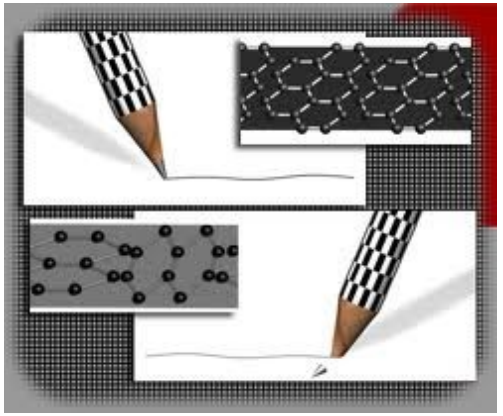

Grafito

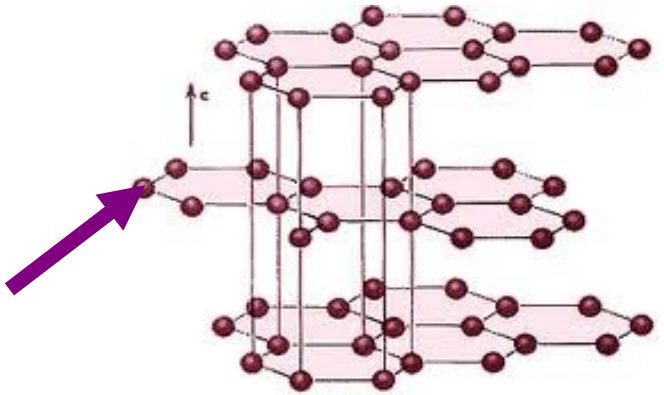

1D

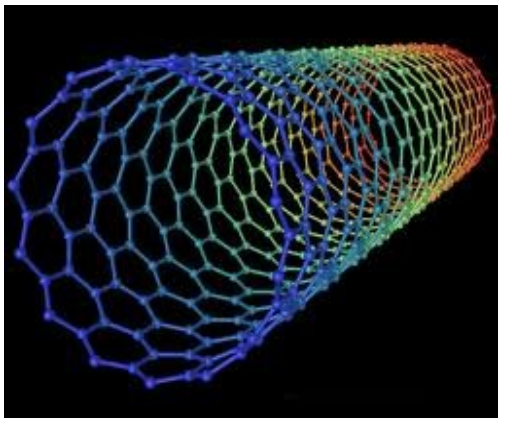

Nanotubos

Diamante

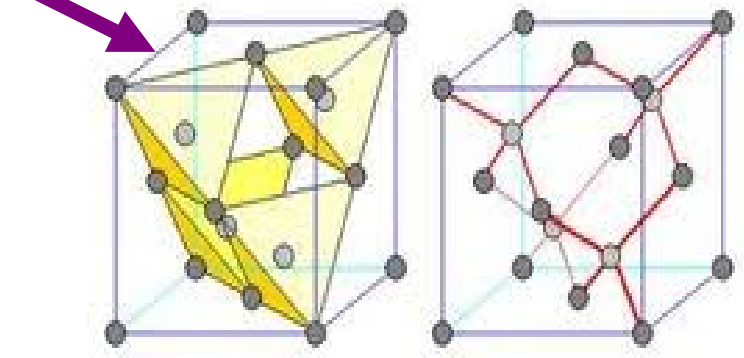

0D

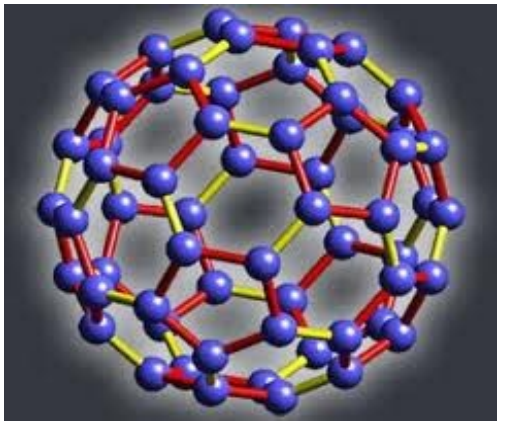

Fulerenos

Breve historia del Carbono

- 1564 Descubrimiento del grafito
- 1779 El grafito es una forma del carbono
- 1789 Nombre griego Υραφειν
- 1960 Inserción de grafito en otros compuestos
- 1985 Fulerenos [Kroto, Curl, Smalley]
- 1991-1994 Nanotubos de Carbono [Iijima]
- 1992-1993 Pocas capas de grafito sobre sustratos metálicos
- 2004 Grafeno esfoliado en sustrato SiO2 [Geim, Novoselov]

Fabricando grafeno con lápiz y cinta Scotch

Electric Field Effect in Atomically Thin Carbon Films

K. S. Novoselov,[1] A. K. Geim,[1]* S. V. Morozov,[2] D. Jiang,[1] Y. Zhang,[1] S. V. Dubonos,[2] I. V. Grigorieva,[1] A. A. Firsov[2]

We describe monocrystalline graphitic films, which are a few atoms thick but are nonetheless stable under ambient conditions, metallic, and of remarkably high quality. The films are found to be a two-dimensional semimetal with a tiny overlap between valence and conductance bands, and they exhibit a strong ambipolar electric field effect such that electrons and holes in concentrations up to 10^{13} per square centimeter and with room-temperature mobilities of ~10,000 square centimeters per volt-second can be induced by applying gate voltage.

The ability to control electronic properties of a material by externally applied voltage is at the heart of modern electronics. In many cases, it is the electric field effect that allows one to vary the carrier concentration in a semiconductor device and, consequently, change an electric current through it. As the semiconductor industry is nearing the limits of performance improvements for the current technologies dominated by silicon, there is a constant search for new, nontraditional materials whose properties can be controlled by the electric field. The most notable recent examples of such materials are organic conductors (*1*) and carbon nanotubes (*2*). It has long been tempting to extend the use of the field effect to metals [e.g., to develop all-metallic transistors that could be scaled down to much smaller sizes and would consume less energy and operate at higher frequencies than traditional semiconducting devices (*3*)]. However, this would require atomically thin metal films, because the electric field is screened at extremely short distances (<1 nm) and bulk carrier concentrations in metals are large compared to the surface charge that can be induced by the field effect. Films so thin tend to be thermodynamically unstable, becoming discontinuous at thicknesses of several nanometers; so far, this has proved to be an insurmountable obstacle to metallic electronics, and no metal or semimetal has been shown to exhibit any notable (>1%) field effect (*4*).

We report the observation of the electric field effect in a naturally occurring two-dimensional (2D) material referred to as few-layer graphene (FLG). Graphene is the name given to a single layer of carbon atoms densely packed into a benzene-ring structure, and is widely used to describe properties of many carbon-based materials, including graphite, large fullerenes, nanotubes, etc. (e.g., carbon nanotubes are usually thought of as graphene sheets rolled up into nanometer-sized cylinders) (*5*–*7*). Planar graphene itself has been presumed not to exist in the free state, being unstable with respect to the formation of curved structures such as soot, fullerenes, and nanotubes (*5*–*14*).

[1]Department of Physics, University of Manchester, Manchester M13 9PL, UK. [2]Institute for Microelectronics Technology, 142432 Chernogolovka, Russia.

*To whom correspondence should be addressed. E-mail: geim@man.ac.uk

be even poorly metallic or continuous under ambient conditions. Using FLG, we demonstrate a metallic field-effect transistor in which the conducting channel can be switched between 2D electron and hole gases by changing the gate voltage.

Our graphene films were prepared by mechanical exfoliation (repeated peeling) of small mesas of highly oriented pyrolytic graphite (*15*). This approach was found to be highly reliable and allowed us to prepare FLG films up to 10 μm in size. Thicker films ($d \geq 3$ nm) were up to 100 μm across and visible by the naked eye. Figure 1 shows examples of the prepared films, including single-layer graphene [see also (*15*)]. To study their electronic properties, we processed the films into multiterminal Hall bar devices placed on top of an oxidized Si substrate so that a gate voltage V_g could be applied. We have studied more than 60 devices with $d < 10$ nm. We focus on the electronic properties of our thinnest (FLG) devices, which contained just one, two, or three atomic layers (*15*). All FLG devices exhibited essentially identical electronic properties characteristic for a 2D semimetal, which differed from a more complex (2D plus 3D) behavior observed for thicker, multilayer graphene (*15*) as well as from the properties of 3D graphite.

In FLG, the typical dependence of its sheet resistivity ρ on gate voltage V_g (Fig. 2) exhibits a sharp peak to a value of several kilohms and decays to ~100 ohms at high V_g (note that 2D resistivity is given in units of ohms rather than ohms × cm as in the 3D case). Its conductivity $\sigma = 1/\rho$ increases linearly with V_g on both sides of the resistivity peak (Fig. 2B). At the same V_g where ρ has its peak, the Hall coefficient R_H exhibits a sharp reversal of its sign (Fig. 2C). The observed behavior resembles the ambipolar field effect in semiconductors, but there is no zero-conductance region associated with the Fermi level being pinned inside the band gap.

Our measurements can be explained quantitatively by a model of a 2D metal with a small overlap δε between conductance and valence bands (*15*). The gate voltage induces a surface charge density $n = \varepsilon_0 \varepsilon V_g / te$ and, accordingly, shifts the position of the Fermi energy ε_F. Here, ε_0 and ε are the permittivities of free space and SiO_2, respectively; e is the electron charge; and t is the thickness of our SiO_2 layer (300 nm). For

theoretical curves. For the regions with only reflecting the fact that R_H is proportional to

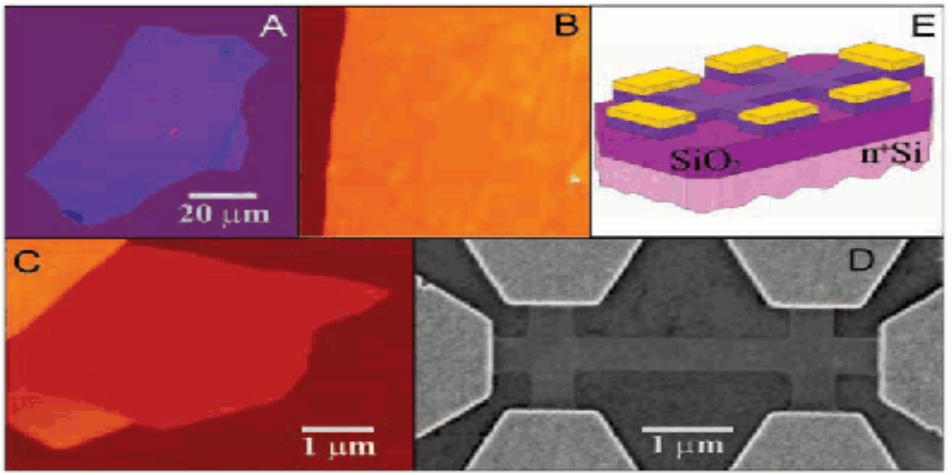

Fig. 1. Graphene films. (**A**) Photograph (in normal white light) of a relatively large multilayer graphene flake with thickness ~3 nm on top of an oxidized Si wafer. (**B**) Atomic force microscope (AFM) image of 2 μm by 2 μm area of this flake near its edge. Colors: dark brown, SiO_2 surface; orange, 3 nm height above the SiO_2 surface. (**C**) AFM image of single-layer graphene. Colors: dark brown, SiO_2 surface; brown-red (central area), 0.8 nm height; yellow-brown (bottom left), 1.2 nm; orange (top left), 2.5 nm. Notice the folded part of the film near the bottom, which exhibits a differential height of ~0.4 nm. For details of AFM imaging of single-layer graphene, see (*15*). (**D**) Scanning electron microscope image of one of our experimental devices prepared from FLG. (**E**) Schematic view of the device in (D).

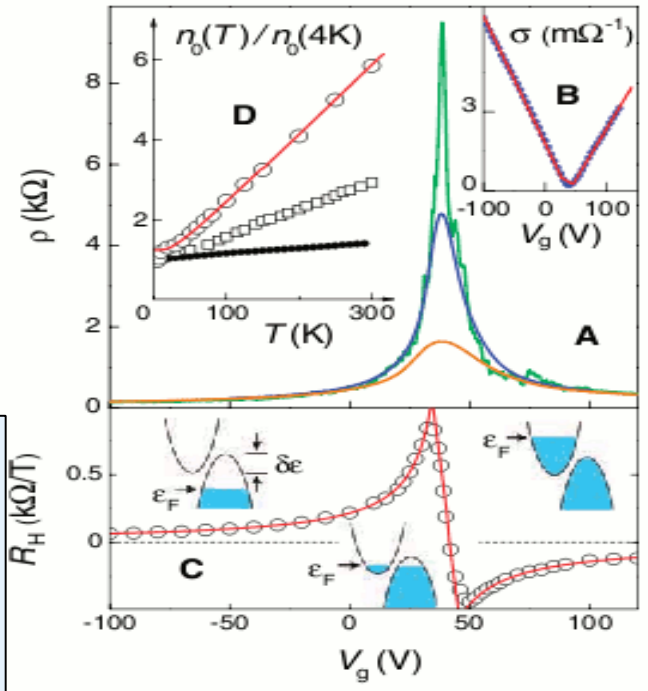

Fig. 2. Field effect in FLG. (**A**) Typical dependences of FLG's resistivity ρ on gate voltage for different temperatures (T = 5, 70, and 300 K for top to bottom curves, respectively). (**B**) Example of changes in the film's conductivity $\sigma = 1/\rho(V_g)$ obtained by inverting the 70 K curve (dots). (**C**) Hall coefficient R_H versus V_g for the same film; T = 5 K. (**D**) Temperature dependence of carrier concentration n_0 in the mixed state for the film in (A) (open circles), a thicker FLG film (squares), and multilayer graphene ($d \approx 5$ nm; solid circles). Red curves in (B) to (D) are the dependences calculated from our model of a 2D semimetal illustrated by insets in (C).

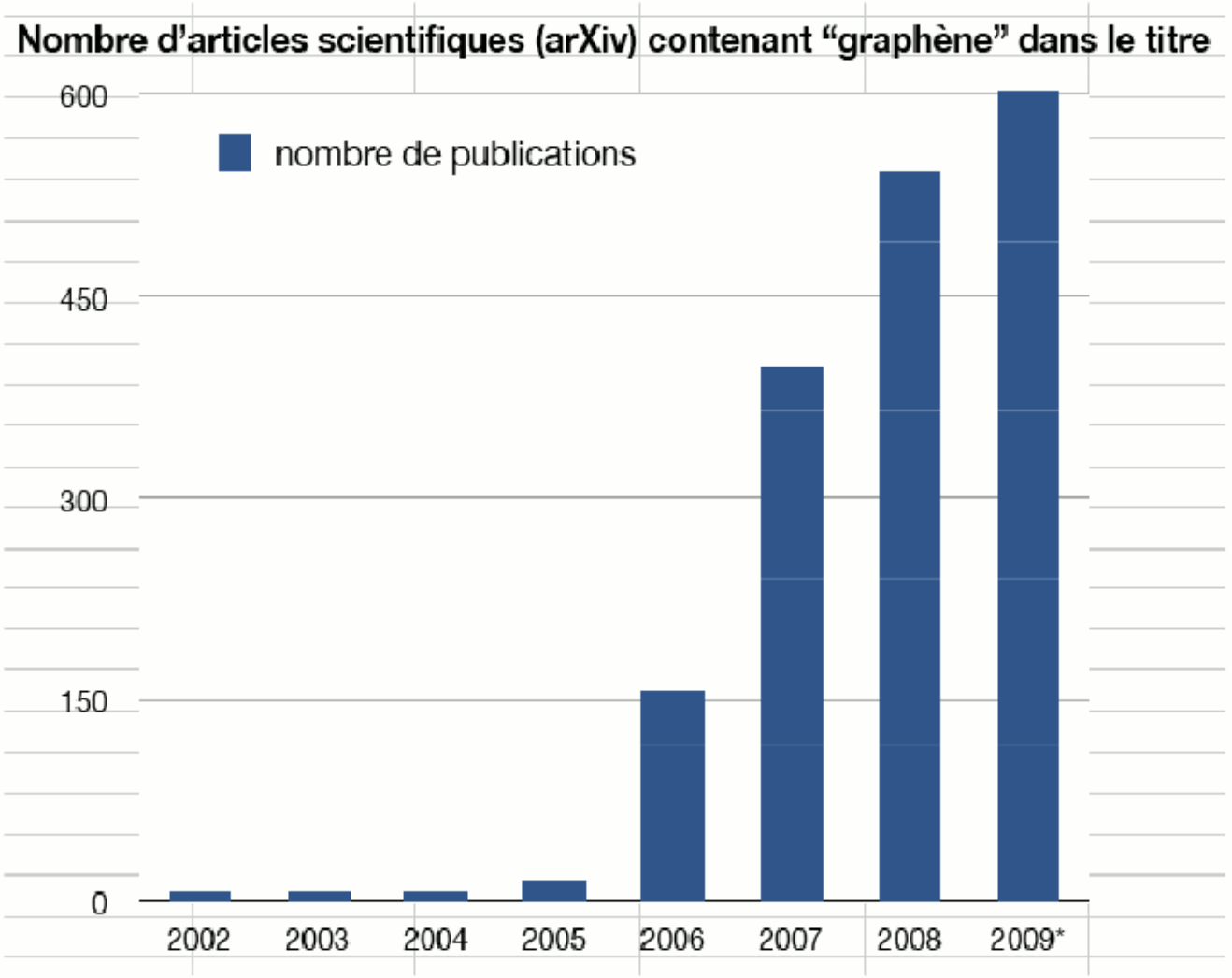

Number of papers on ArXiv with the key word « graphene »

http://www.condmat.physics.manchester.ac.uk/people/academic/geim/

- *F. Guinea, M. I. Katsnelson & A. K. Geim* Energy gaps and a zero-field quantum Hall effect in graphene by strain engineering ***Nature Physics 6***, 30-33 (2010).
- *A. K. Geim* Graphene: Status and Prospects ***Science 324***, 1530-1534 (2009).
- *D. C. Elias, R. R. Nair, T. M. G. Mohiuddin, S. V. Morozov, P. Blake, M. P. Halsall, A. C. Ferrari, D. W. Boukhvalov, M. I. Katsnelson, A. K. Geim & K. S. Novoselov* Control of Graphene's Properties by Reversible Hydrogenation: Evidence for Graphane ***Science* 323**, 610-613 (2009).
- *A. H. Castro Neto, F. Guinea, N. M. R. Peres, K. S. Novoselov & A. K. Geim* The Electronic Properties of Graphene ***Reviews of Modern Physics* 81**, 109-162 (2009).
- *Mhairi H. Gass, Ursel Bangert, Andrew L. Bleloch, Peng Wang, Rahul R. Nair & A. K. Geim* Free-Standing Graphene at Atomic Resolution ***Nature Nanotechnology* 3**, 676-681 (2008).
- *R. R. Nair, P. Blake, A. N. Grigorenko, K. S. Novoselov, T. J. Booth, T. Stauber, N. M. R. Peres, & A. K. Geim* Fine Structure Constant Defines Visual Transparency of Graphene ***Science* 320**, 1308 (2008).
- *L. A. Ponomarenko, F. Schedin, M. I. Katsnelson, R. Yang, E. W. Hill, K. S. Novoselov & A. K. Geim* Chaotic Dirac Billiard in Graphene Quantum Dots ***Science* 320**, 356-358 (2008).
- *A.K. Geim & P. Kim* Carbon Wonderland ***Scientific American*** 90-97, April 2008.
- *A. Das, S. Pisana, B. Chakraborty, S. Piscanec, S. K. Saha, U. V. Waghmare, K. S. Novoselov, H. R. Krishnamurthy, A. K. Geim, A. C. Ferrari & A. K. Sood* Monitoring Dopants by Raman Scattering in an Electrochemically Top-Gated Graphene Transistor ***Nature Nanotechnology* 3**, 210-215 (2008).
- *A.K. Geim & A.H. MacDonald* Graphene: Exploring Carbon Flatland ***Physics Today* 60**, 35-41 (2007).
- *K.S. Novoselov, Z. Jiang, Y. Zhang, S.V. Morozov, H.L. Stormer, U. Zeitler, J.C. Maan, G.S. Boebinger, P. Kim & A.K. Geim* Room-Temperature Quantum Hall Effect in Graphene ***Science* 315**, 1379 (2007).
- *J.C. Meyer, A.K. Geim, M.I. Katsnelson, K.S. Novoselov, T.J. Booth & S. Roth* The Structure of Suspended Graphene Sheets ***Nature* 446**, 60-63 (2007).
- *A.K. Geim & K.S. Novoselov* The Rise of Graphene ***Nature Materials* 6**, 183-191 (2007).

http://www.condmat.physics.manchester.ac.uk/people/academic/geim/

- *F. Schedin, A.K. Geim, S. V. Morozov, E. W. Hill, P. Blake, M. I. Katsnelson & K.S. Novoselov* Detection of Individual Gas Molecules Adsorbed on Graphene ***Nature Materials* 6**, 652-655 (2007).
- *S. Pisana, M. Lazzeri, C. Casiraghi, K.S. Novoselov, A.K. Geim, A.C. Ferrari & F. Mauri* Breakdown of the Adiabatic Born–Oppenheimer Approximation in Graphene ***Nature Materials* 6**, 198-201 (2007).
- *M.I. Katsnelson, K.S. Novoselov & A.K. Geim* Chiral Tunnelling and the Klein Paradox in Graphene ***Nature Physics* 2**, 620-625 (2006).
- *K.S. Novoselov, E. McCann, S.V. Morozov, V.I. Fal'ko, M.I. Katsnelson, U. Zeitler, D. Jiang, F. Schedin & A.K. Geim* Unconventional Quantum Hall Effect and Berry's Phase of 2π in Bilayer Graphene ***Nature Physics* 2**, 177-180 (2006).
- *K.S. Novoselov, A.K. Geim, S.V.Morozov, D.Jiang, M.I.Katsnelson, I.V.Grigorieva, S.V.Dubonos & A.A.Firsov* Two-Dimensional Gas of Massless Dirac Fermions in Graphene ***Nature* 438**, 197-200 (2005).
- *K.S. Novoselov, D. Jiang, F. Schedin, T. Booth, V.V. Khotkevich, S.V. Morozov & A.K. Geim.* Two Dimensional Atomic Crystals ***PNAS* 102**, 10451-10453 (2005).
- *K.S. Novoselov, A.K. Geim, S.V. Morozov, D. Jiang, Y. Zhang, S.V. Dubonos, I.V. Grigorieva, & A.A. Firsov.* Electric Field Effect in Atomically Thin Carbon Films ***Science* 306**, 666-669 (2004).

Potencial tecnológico del grafeno

- Alta conductividad eléctrica y térmica.
- Alta elasticidad y dureza.
- 200 veces más resistente que el acero.
- Baja disipación de energía por efecto Joule.
- Liviano.
- Resistente a la radiación.

Física fundamental del grafeno

REVIEW

Graphene: Status and Prospects

A. K. Geim Science 324, 530 (2009)

Graphene is a wonder material with many superlatives to its name. It is the thinnest known material in the universe and the strongest ever measured. Its charge carriers exhibit giant intrinsic mobility, have zero effective mass, and can travel for micrometers without scattering at room temperature. Graphene can sustain current densities six orders of magnitude higher than that of copper, shows record thermal conductivity and stiffness, is impermeable to gases, and reconciles such conflicting qualities as brittleness and ductility. Electron transport in graphene is described by a Dirac-like equation, which allows the investigation of relativistic quantum phenomena in a benchtop experiment. This review analyzes recent trends in graphene research and applications, and attempts to identify future directions in which the field is likely to develop.

Sistema de N electrones no relativistas

$$H = \sum_l H_l = \sum_l \left[\frac{-\hbar^2 \nabla_l^2}{2m} \right]$$ Libres

$$H = \sum_l \left[\frac{-\hbar^2 \nabla_l^2}{2m} \right] + \sum_{l,i} V(\vec{r}_l - \vec{R}_i)$$ En el sólido

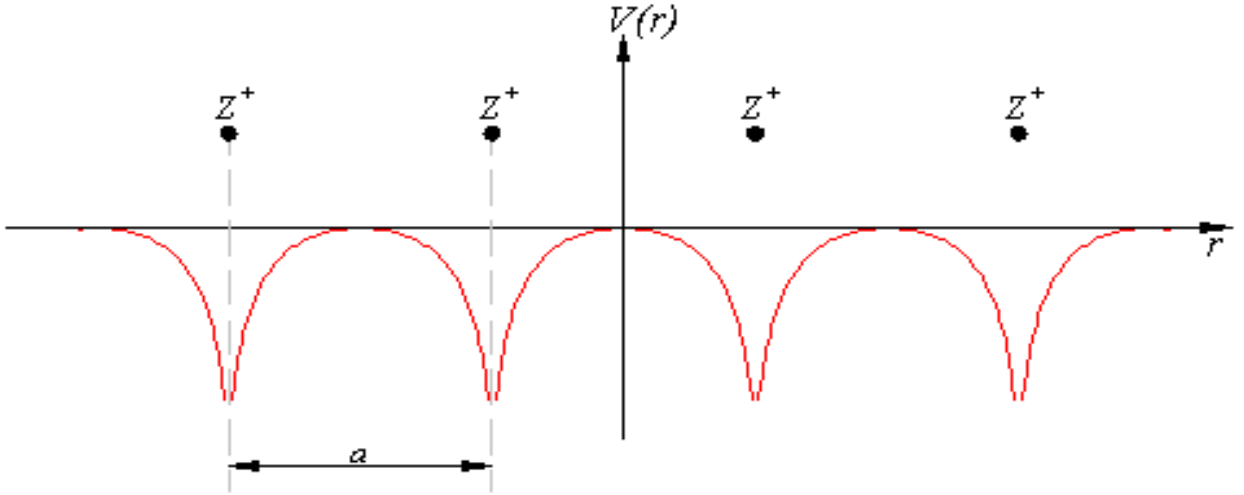

Solución de la ecuación de Schrödinger para electrones libres no relativistas

Estado fundamental de N e-

$$\Psi_k(\vec{r}_l) = \frac{1}{\sqrt{L^3}} e^{i\vec{k}.\vec{r}_l}$$

$$H_l \Psi_k(\vec{r}_l) = \varepsilon_k \Psi_k(\vec{r}_l)$$

$$\varepsilon_k = \frac{\hbar^2 k^2}{2m}$$

Relación de dispersión

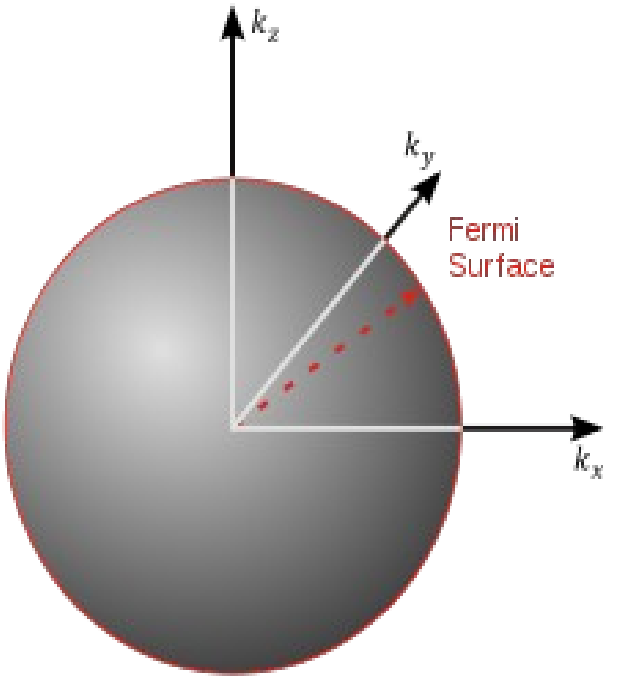

$$\vec{k} = \frac{2\pi}{L}(n_x, n_y, n_z), n_i \notin \mathbb{Z}$$

Graphene electronic structure

Graphene = 2D honeycomb carbon crystal

Carbon: 6 electrons $1s^2$, $2s^2$ $2p^2$
hybridation: 1 orbital 2s and 2 orbitals 2p
→ 3 orbitals sp^2
-3 coplanar σ bonds, angle 120°:
→honeycomb structure
→covalent bonding

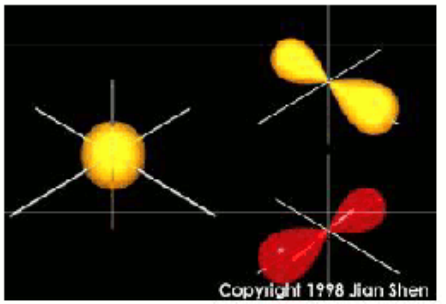

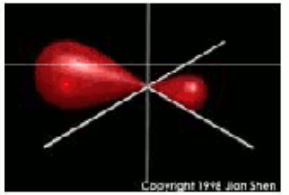

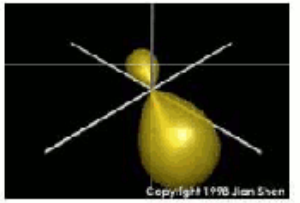

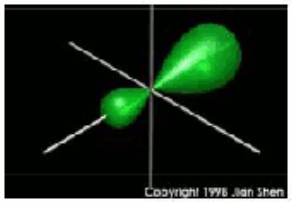

+ 1 orbital $2p_z$ perpendicular to the plane

→ 1 conduction e per C

→ Half-filled band

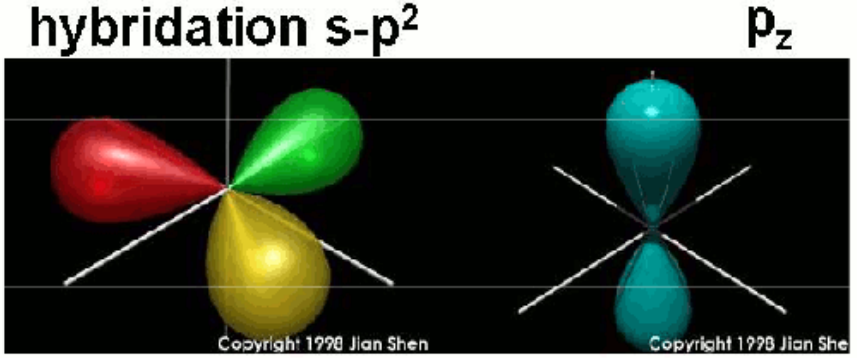

« Honeycomb lattice » is not a Bravais lattice

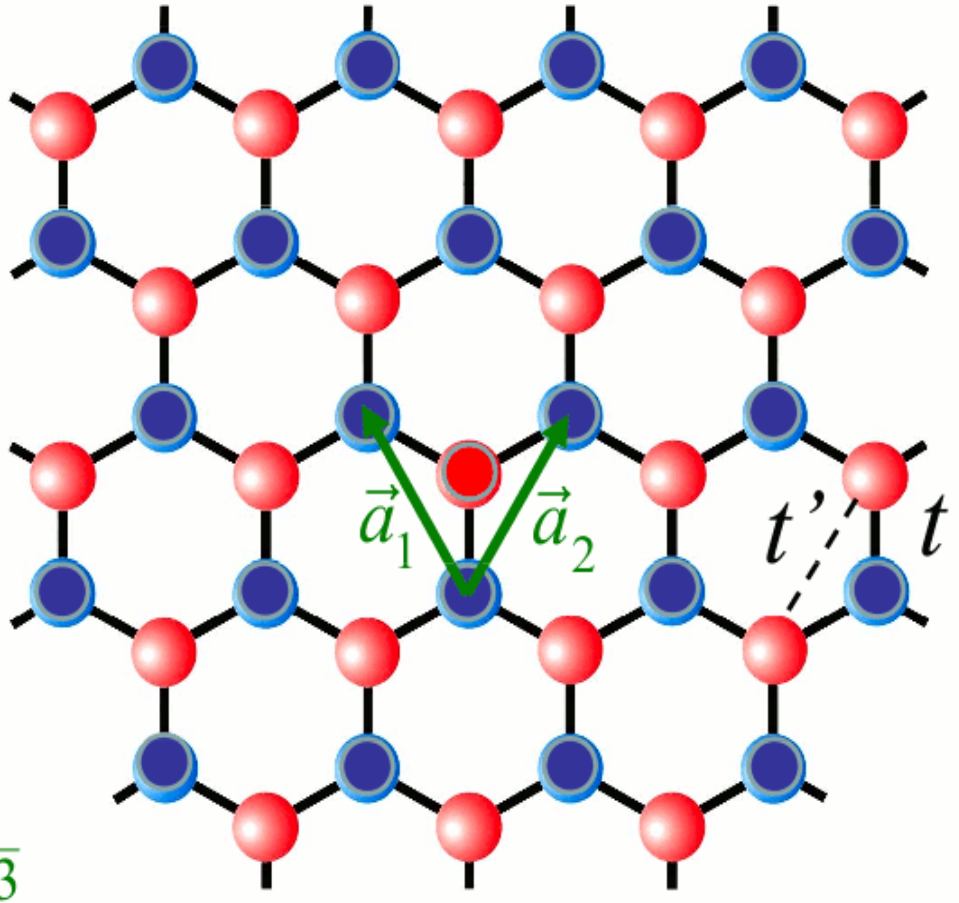

a=1.42 A

$t=2.8eV$

$t'=-0.2eV$

$a_0 = |\vec{a}_1| = a\sqrt{3}$

a = C-C distance
a_0 = lattice parameter

Triangular Bravais lattice + 2 atoms per unit cell

Real Space

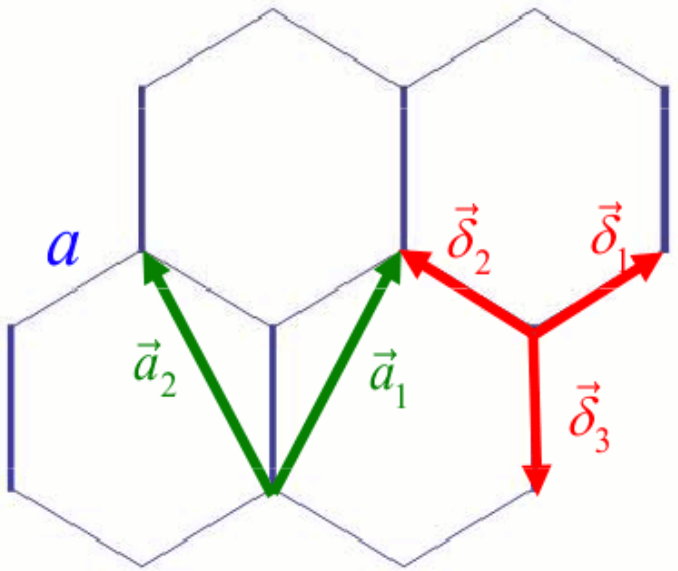

Triangular Bravais lattice
+ 2 identical atoms per unit cell

$$a = 0.142nm$$

Reciprocal space

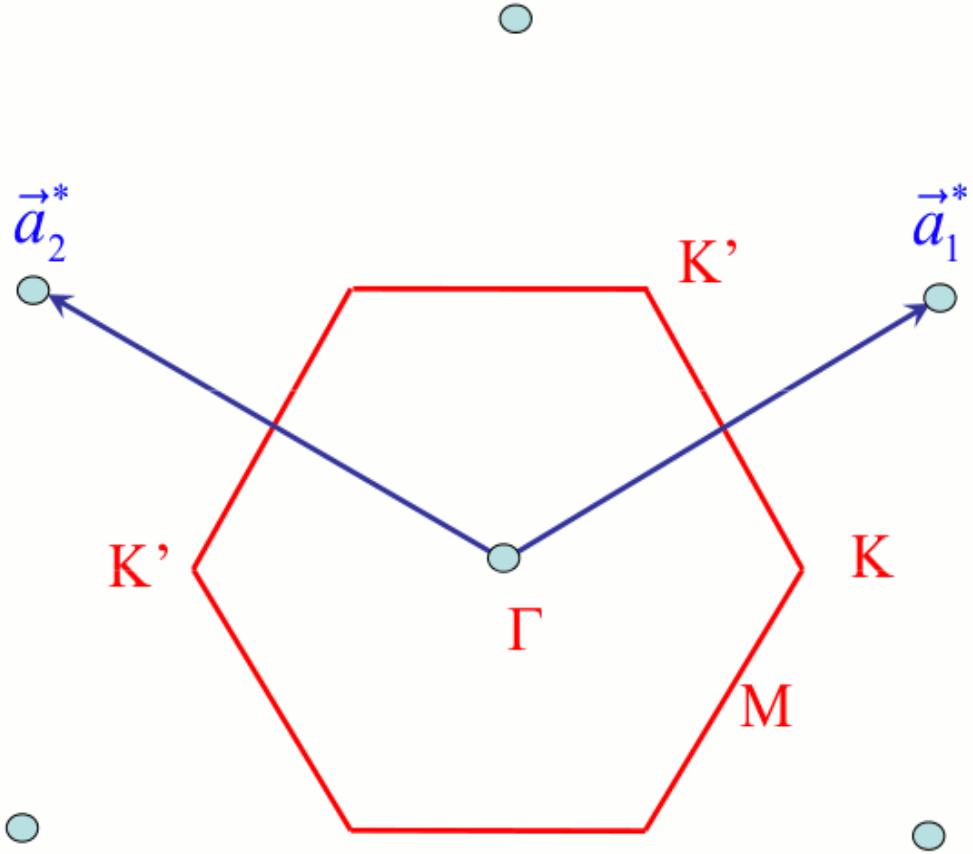

$$\vec{K} = \pm\frac{1}{3}(\vec{a}_1^* - \vec{a}_2^*) + \vec{G}$$

$$\left|a_i^*\right| = \frac{4\pi}{3a} \qquad \Gamma K = KK' = \frac{4\pi}{3\sqrt{3}a}$$

Nearest neighbor tight-binding model for the conduction electrons, Wallace 1947

Nearest neighbor hopping t

1 conduction electron per atom

(next nearest hopping t')

$$H = -t\sum_{j,j'}\left|\varphi_A^j\right\rangle\left\langle\varphi_B^{j'}\right| + h.c$$

$$-t'\sum_{j,j'}\left(\left|\varphi_A^j\right\rangle\left\langle\varphi_A^{j'}\right| + \left|\varphi_B^j\right\rangle\left\langle\varphi_B^{j'}\right|\right) + h.c$$

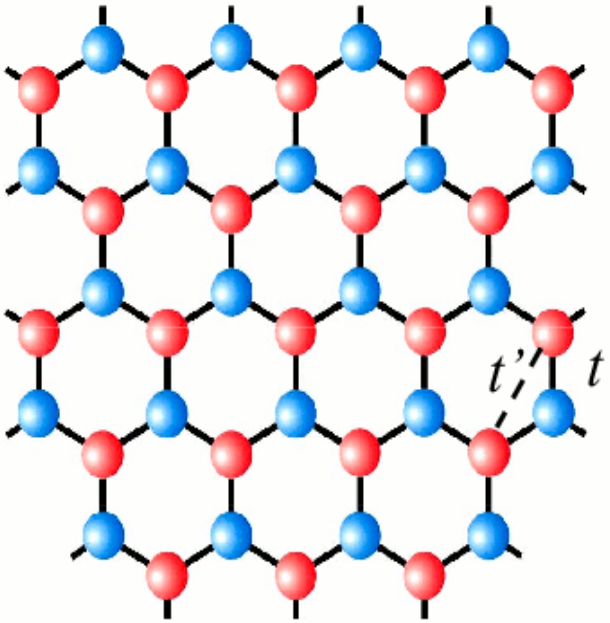

+ Bloch theorem ....

$$|\psi\rangle = \frac{1}{\sqrt{N}} \sum_{cells} e^{i\vec{k}\cdot\vec{R}_j} \left[c_A(\vec{k}) \left|\varphi_A^j\right\rangle + c_B(\vec{k}) \left|\varphi_B^j\right\rangle \right]$$

$$\begin{pmatrix} 0 & f(\vec{k}) \\ f^*(\vec{k}) & 0 \end{pmatrix} \begin{pmatrix} c_A(\vec{k}) \\ c_B(\vec{k}) \end{pmatrix} = E \begin{pmatrix} c_A(\vec{k}) \\ c_B(\vec{k}) \end{pmatrix}$$

$$f(\vec{k}) = -t(1 + e^{-i\vec{k}\cdot\vec{a}_1} + e^{-i\vec{k}\cdot\vec{a}_2})$$

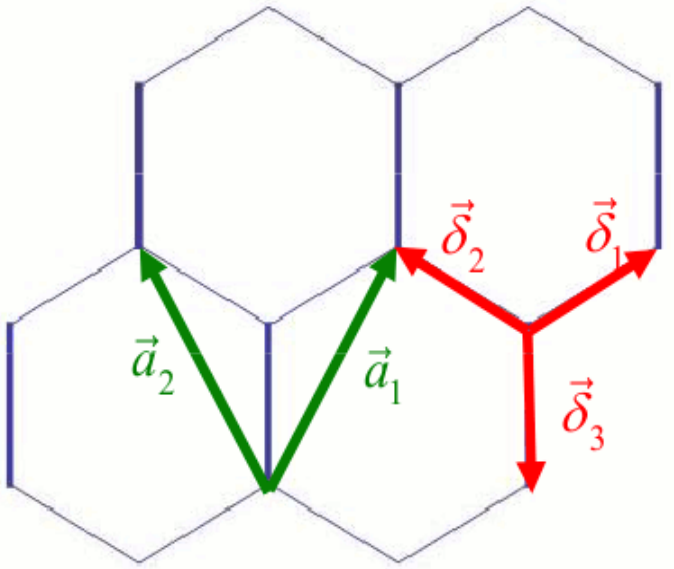

$$\begin{pmatrix} 0 & f'(\vec{k}) \\ f'^*(\vec{k}) & 0 \end{pmatrix} \begin{pmatrix} d_A(\vec{k}) \\ d_B(\vec{k}) \end{pmatrix} = E \begin{pmatrix} d_A(\vec{k}) \\ d_B(\vec{k}) \end{pmatrix}$$

$$f'(\vec{k}) = -t(e^{-i\vec{k}\cdot\vec{\delta}_3} + e^{-i\vec{k}\cdot\vec{\delta}_1} + e^{-i\vec{k}\cdot\vec{\delta}_2})$$

$$|\psi\rangle = \frac{1}{\sqrt{N}} \sum_{cells} \left[d_A(\vec{k}) e^{i\vec{k}\cdot\vec{R}_j^A} \left|\varphi_A^j\right\rangle + d_B(\vec{k}) e^{i\vec{k}\cdot\vec{R}_j^B} \left|\varphi_B^j\right\rangle \right]$$

C. Bena, G.M.,
New. J. Phys. 11, 095003 (2009)

Ver también ejercicio de C.Schönenberger, E2 (2009) df.uba.ar

Energy spectum

$$f(\vec{k}) = -t(1 + e^{-i\vec{k}\cdot\vec{a}_1} + e^{-i\vec{k}\cdot\vec{a}_2})$$

$$E(\vec{k}) = \pm\left|f(\vec{k})\right|$$

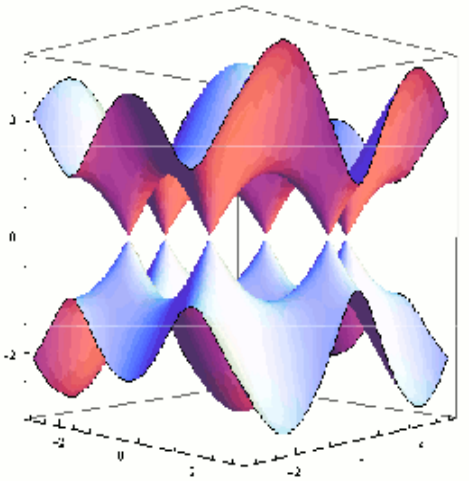

$$E(\vec{k}) = \pm\left|f(\vec{k})\right| - 2t'[\cos\vec{k}.\vec{a}_1 + \cos\vec{k}.\vec{a}_2 + \cos\vec{k}.(\vec{a}_1 - \vec{a}_2)]$$

$t = 2.8\,eV$

$t' = -0.2\,eV$

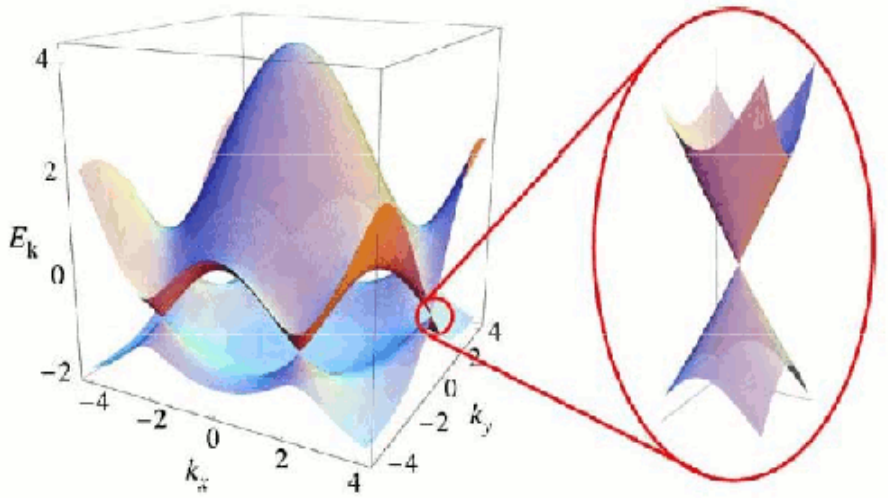

Expansion near the Dirac points

$$f(\pm\vec{K}+\vec{q}) = c(\pm q_x - iq_y)$$

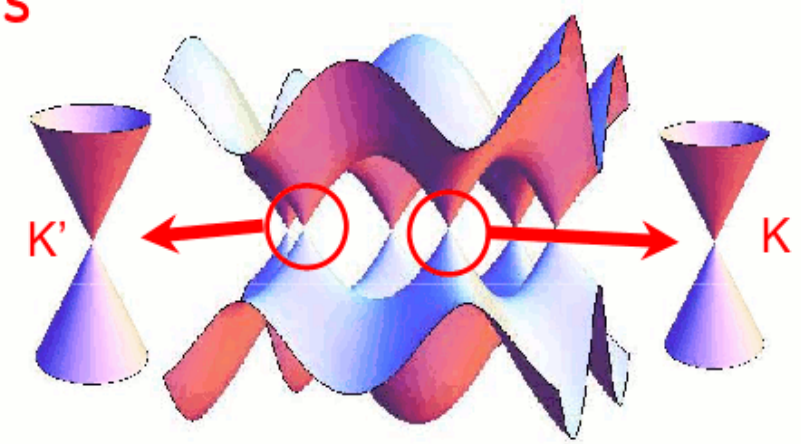

$$H_{\substack{K\\K'}} = c\begin{pmatrix} 0 & \pm q_x - iq_y \\ \pm q_x + iq_y & 0 \end{pmatrix}$$

2+1 Dirac eq.

$$c \equiv v_F = \frac{3}{2}ta$$

$$H^2\psi = \varepsilon^2\psi$$

$$H_K^2 = c^2\begin{pmatrix} q_x^2+q_y^2 & 0 \\ 0 & q_x^2+q_y^2 \end{pmatrix}$$

How to write the effective linearized Hamiltonian

$$H_{K,K'} = c\begin{pmatrix} 0 & \pm q_x - iq_y \\ \pm q_x + iq_y & 0 \end{pmatrix} = c(\pm q_x \sigma_x + q_y \sigma_y)$$

$$H = c\begin{pmatrix} \text{A} & \text{B} & \text{A}' & \text{B}' \\ 0 & q_x - iq_y & 0 & 0 \\ q_x + iq_y & 0 & 0 & 0 \\ 0 & 0 & 0 & -q_x - iq_y \\ 0 & 0 & -q_x + iq_y & 0 \end{pmatrix}$$

4 x 4 effective Hamiltonian

Two uncoupled valleys

$$H = c\begin{pmatrix} \text{A} & \text{B} & \text{B}' & \text{A}' \\ 0 & q_x - iq_y & 0 & 0 \\ q_x + iq_y & 0 & 0 & 0 \\ 0 & 0 & 0 & -q_x + iq_y \\ 0 & 0 & -q_x - iq_y & 0 \end{pmatrix} = c\,\vec{q}.\vec{\sigma} \otimes \tau_z$$

A. Geim, Science 324, 530 (2009)

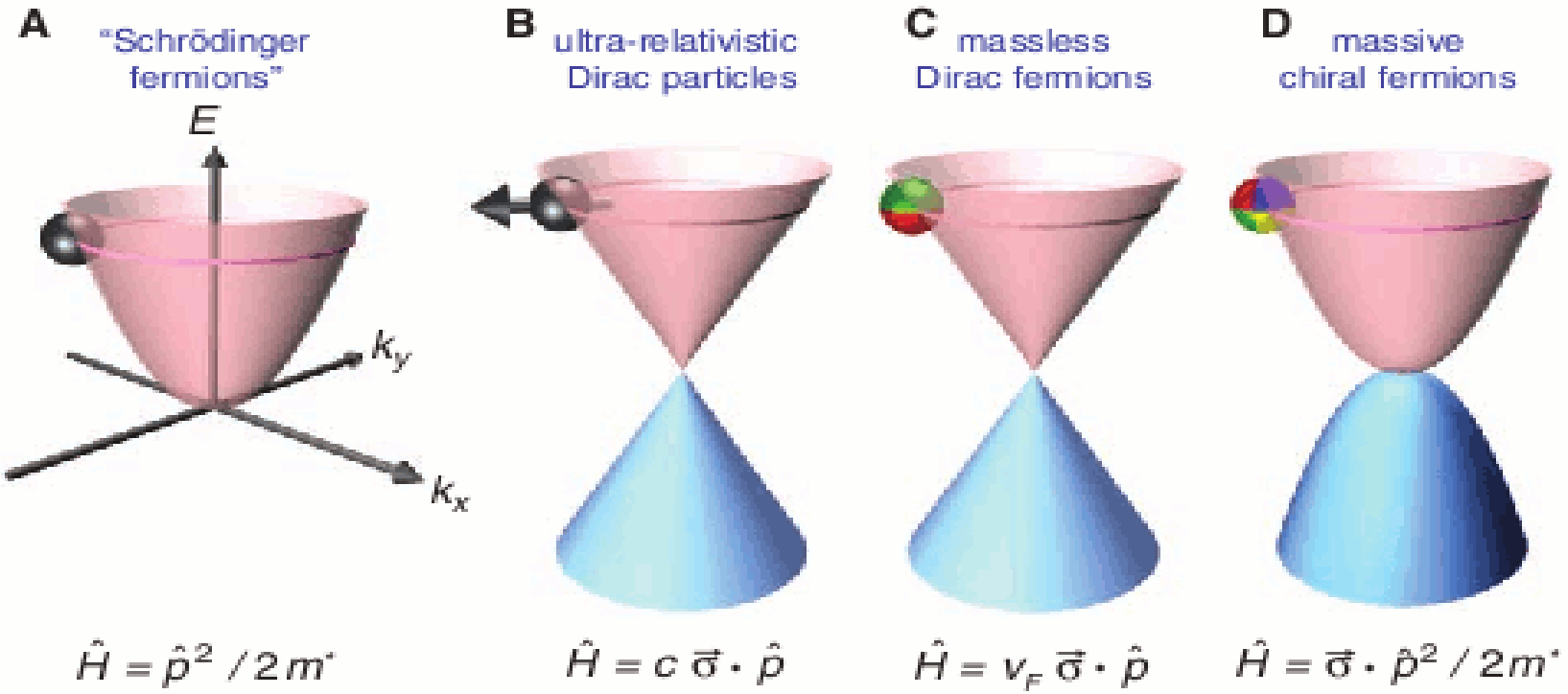

Fig. 2. Quasi-particle zoo. (**A**) Charge carriers in condensed matter physics are normally described by the Schrödinger equation with an effective mass m^* different from the free electron mass ($\hat{p}$ is the momentum operator). (**B**) Relativistic particles in the limit of zero rest mass follow the Dirac equation, where c is the speed of light and $\vec{\sigma}$ is the Pauli matrix. (**C**) Charge carriers in graphene are called massless Dirac fermions and are described by a 2D analog of the Dirac equation, with the Fermi velocity $v_F \approx 1 \times 10^6$ m/s playing the role of the speed of light and a 2D pseudospin matrix $\vec{\sigma}$ describing two sublattices of the honeycomb lattice (*3*). Similar to the real spin that can change its direction between, say, left and right, the pseudospin is an index that indicates on which of the two sublattices a quasi-particle is located. The pseudospin can be indicated by color (e.g., red and green). (**D**) Bilayer graphene provides us with yet another type of quasi-particles that have no analogies. They are massive Dirac fermions described by a rather bizarre Hamiltonian that combines features of both Dirac and Schrödinger equations. The pseudospin changes its color index four times as it moves among four carbon sublattices (*2*–*4*).

Efectos interesantes

M. I. Kastnelson, K. Novoselon and A. Geim,''Klein paradox and chiral tunneling in graphene'' Nature Phys 2, 620 (2006)

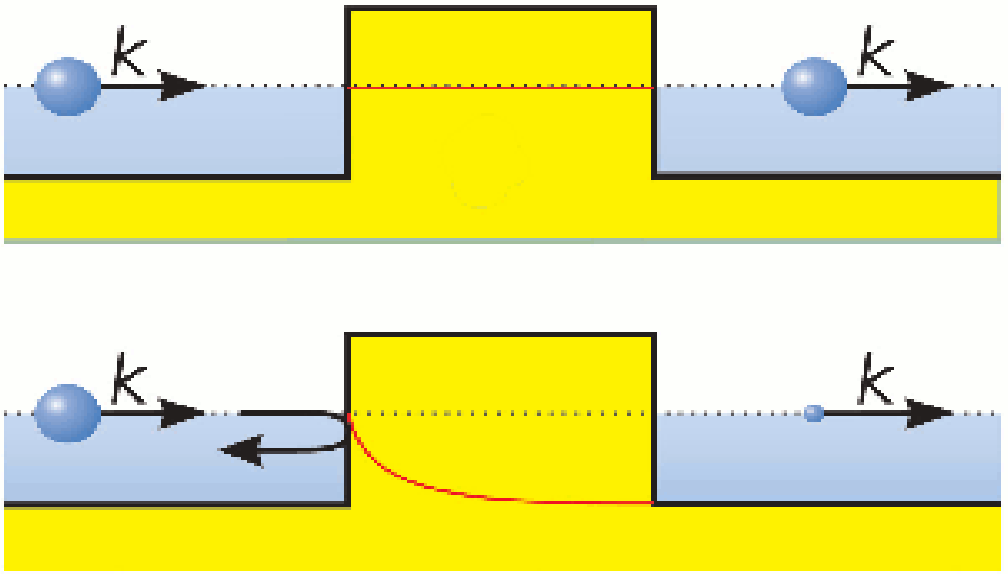

Fig. 9 Tunneling in graphene (top) and conventional semiconductors (bottom). The amplitude of the electron wave function (red) remains constant in graphene while it decays exponentially in conventional tunneling. The size of the sphere indicates the amplitude of the incident and transmitted wave functions. (Reprinted with permission from[50]. © 2006 Nature Publishing Group.)

Klein tunneling effect

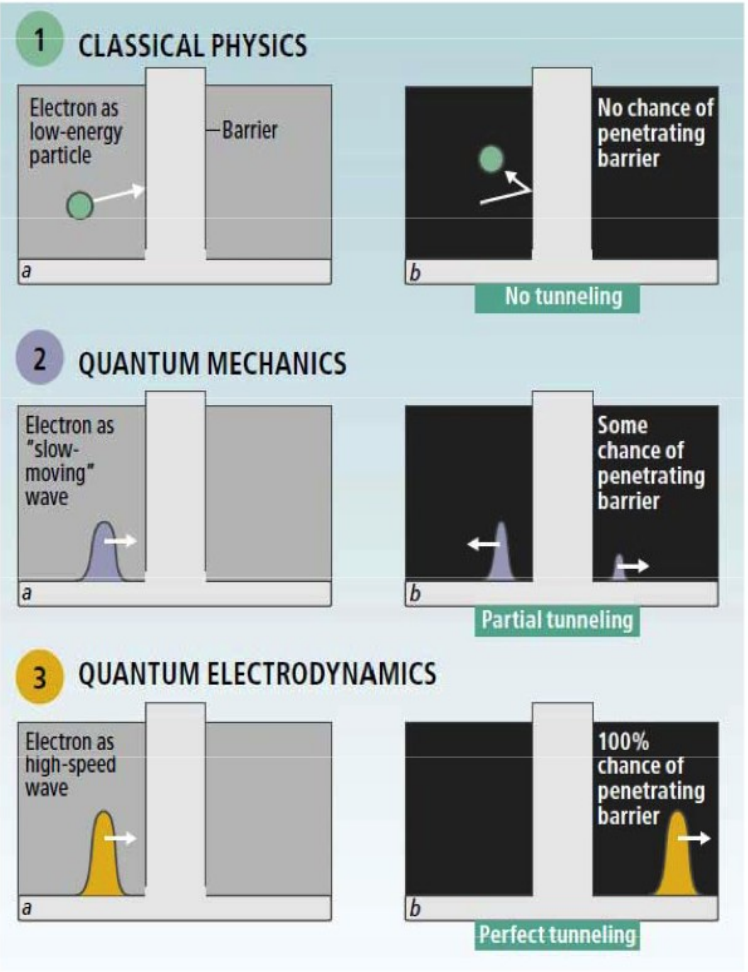

Oskar Klein (1894-1977)

Die Reflexion von Elektronen an einem Potentialsprung nach der relativistischen Dynamik von Dirac.

Von **O. Klein** in Kopenhagen.

(Eingegangen am 24. Dezember 1928.)

$E = \frac{p_x^2}{2m}$

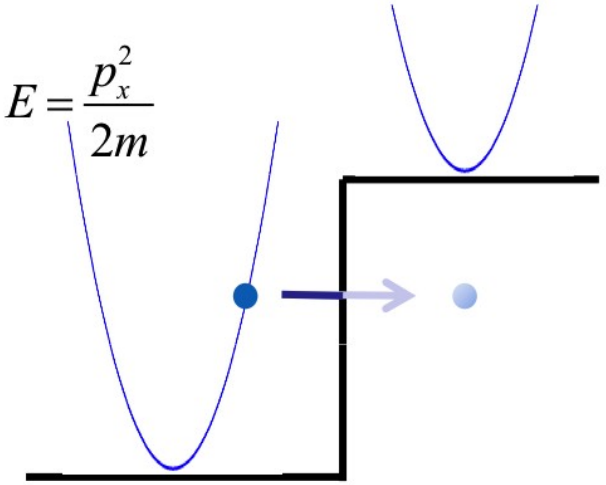

$E = c|p_x|$

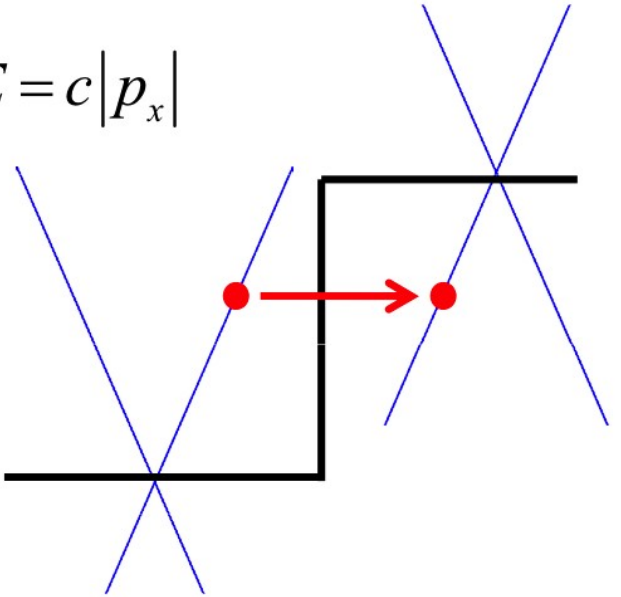

$E = \sqrt{p_x^2 c^2 + m^2 c^4}$

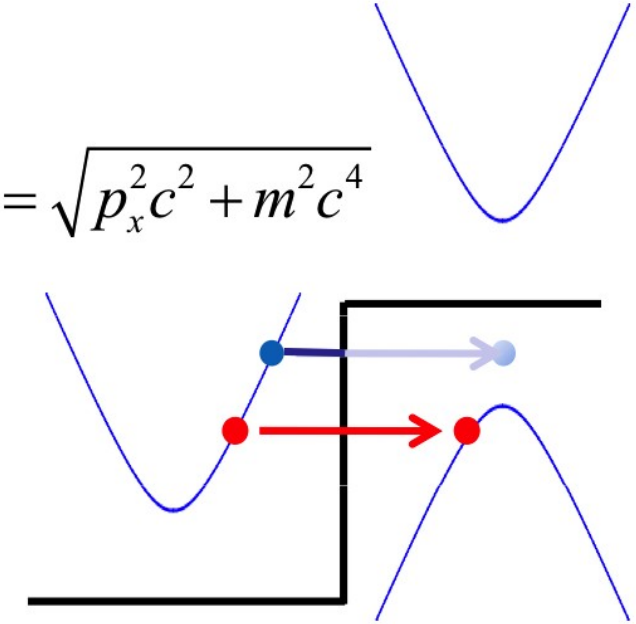

Evanescent mode

Transmission

Potential step

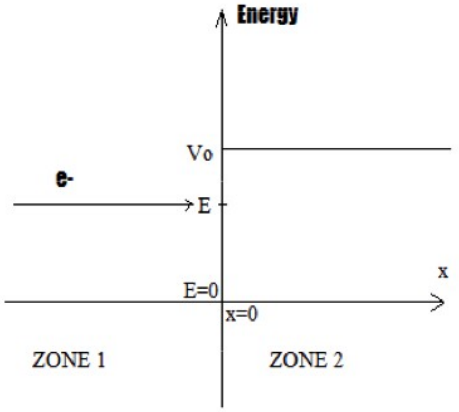

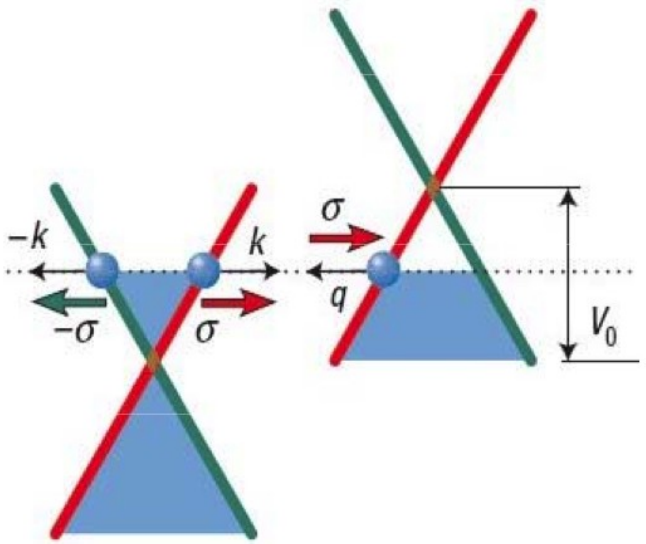

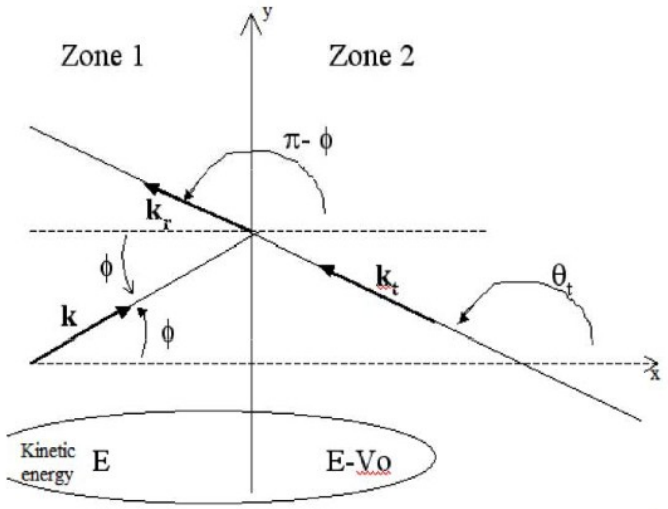

$$\psi_I(\boldsymbol{r}) = \frac{1}{\sqrt{2}}\begin{pmatrix}1\\ se^{i\phi}\end{pmatrix}e^{i(k_x x+k_y y)} + \frac{r}{\sqrt{2}}\begin{pmatrix}1\\ se^{i(\pi-\phi)}\end{pmatrix}e^{i(-k_x x+k_y y)}$$

$$\psi_{II}(\boldsymbol{r}) = \frac{a}{\sqrt{2}}\begin{pmatrix}1\\ s'e^{i\theta}\end{pmatrix}e^{i(q_x x+k_y y)}$$

+ Continuity equations →

$$T(\phi) = -\frac{\cos\phi\cos\theta_t}{\sin^2\left(\frac{\phi+\theta_t}{2}\right)}$$

$$E\sin\phi = (V_0 - E)\sin\theta_t$$

Potential barrier

$$\psi_I(\boldsymbol{r}) = \frac{1}{\sqrt{2}}\begin{pmatrix} 1 \\ se^{i\phi} \end{pmatrix} e^{i(k_x x + k_y y)} + \frac{r}{\sqrt{2}}\begin{pmatrix} 1 \\ se^{i(\pi-\phi)} \end{pmatrix} e^{i(-k_x x + k_y y)}$$

$$\psi_{\mathrm{II}}(\boldsymbol{r}) = \frac{a}{\sqrt{2}}\begin{pmatrix} 1 \\ s'e^{i\theta} \end{pmatrix} e^{i(q_x x + k_y y)} + \frac{b}{\sqrt{2}}\begin{pmatrix} 1 \\ s'e^{i(\pi-\theta)} \end{pmatrix} e^{i(-q_x x + k_y y)}$$

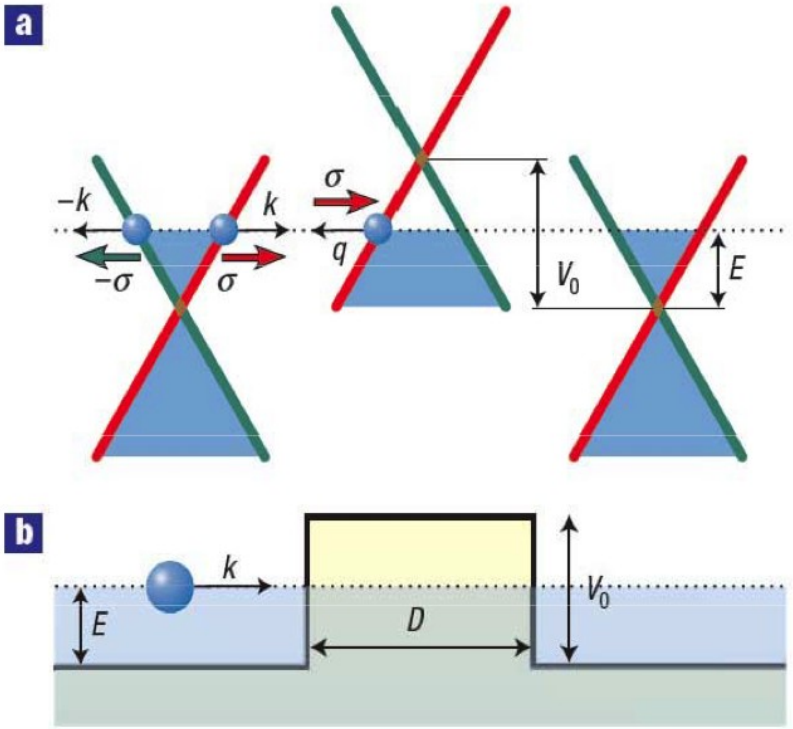

$$\psi_{\mathrm{III}}(\boldsymbol{r}) = \frac{t}{\sqrt{2}}\begin{pmatrix} 1 \\ se^{i\phi} \end{pmatrix} e^{i(k_x x + k_y y)}$$

+ Continuity equations
→

Potential barrier

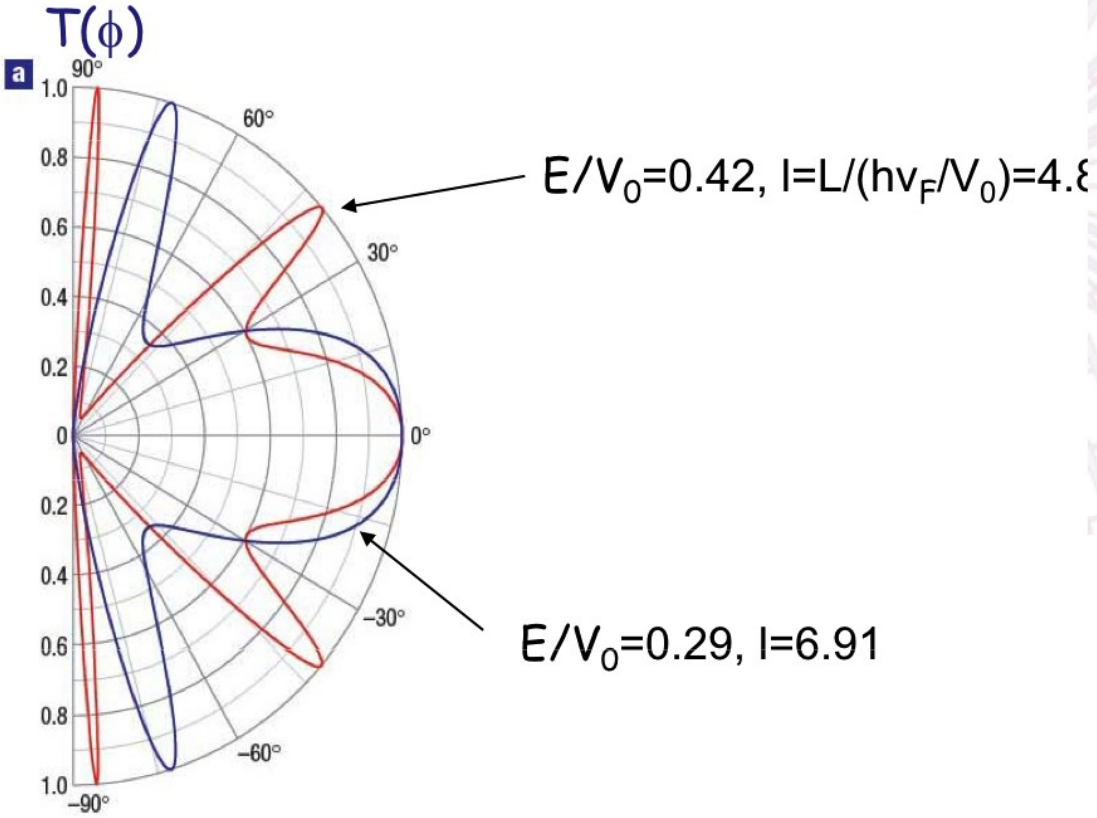

Katsnelson, Novoselov and Geim, Nat. Phys. 2, 620 (2006)

$$E\sin\phi = (V_0 - E)\sin\theta_t$$

$$q_x = (V_0 - E)\cos\theta_t$$

$$T(\phi) = \frac{\cos^2\phi\cos^2\theta_t}{\cos^2 q_x L\cos^2\phi\cos^2\theta_t + \sin^2 q_x L\,(1+\sin\phi\sin\theta_t)^2}$$

Science, 320 (2008)

Fine Structure Constant Defines Visual Transparency of Graphene

R. R. Nair,[1] P. Blake,[1] A. N. Grigorenko,[1] K. S. Novoselov,[1] T. J. Booth,[1] T. Stauber,[2] N. M. R. Peres,[2] A. K. Geim[1]*

There are few phenomena in condensed matter physics that are defined only by the fundamental constants and do not depend on material parameters. Examples are the resistivity quantum, h/e^2, that appears in a variety of transport experiments, including the quantum Hall effect and universal conductance fluctuations, and the magnetic flux quantum, $h/2e$, playing an important role in the physics of superconductivity (h is Planck's constant and e the electron charge). By and large, it requires sophisticated facilities and special measurement conditions to observe any of these phenomena. In contrast, we show that the opacity of suspended graphene (1) is defined solely by the fine structure constant, $\alpha = e^2/\hbar c \approx 1/137$ (where c is the speed of light), the parameter that describes coupling between light and relativistic electrons and that is traditionally associated with quantum electrodynamics rather than materials science. Despite being only one atom thick, graphene is found to absorb a significant ($\pi\alpha$ = 2.3%) fraction of incident white light, a consequence of graphene's unique electronic structure.

We have studied specially prepared graphene crystals (*5*) such that they covered submillimeter apertures in a metal scaffold (Fig. 1A inset). Such large one-atom-thick membranes suitable for (E < 1 eV), beyond which the electronic spectrum of graphene becomes strongly warped and nonlinear and the approximation of Dirac fermions breaks down. However, our calculations (*5*) show that finite-E corrections are surprisingly small (a few %) even for visible light. Because of these corrections, a metrological accuracy for α would be difficult to achieve, but it is remarkable that the fine structure constant can so directly be assessed practically by the naked eye.

References and Notes

1. A. K. Geim, K. S. Novoselov, *Nat. Mater.* **6**, 183 (2007).
2. T. Ando, Y. Zheng, H. Suzuura, *J. Phys. Soc. Jpn.* **71**, 1318 (2002).
3. V. P. Gusynin, S. G. Sharapov, J. P. Carbotte, *Phys. Rev. Lett.* **96**, 256802 (2006).

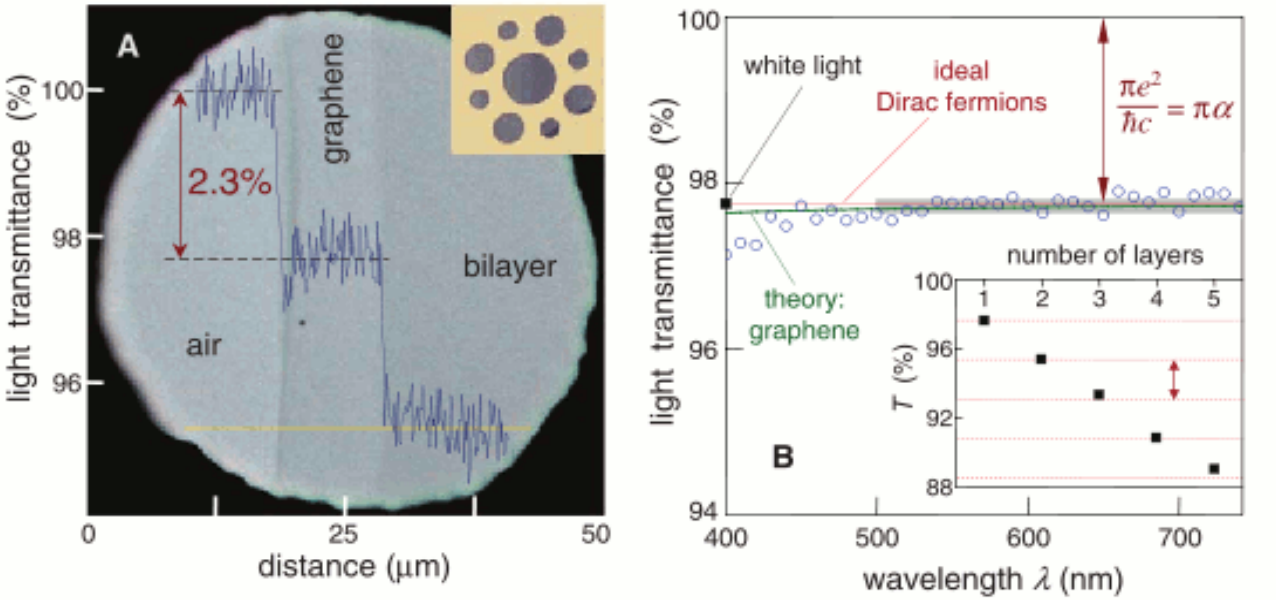

Fig. 1. Looking through one-atom-thick crystals. (**A**) Photograph of a 50-μm aperture partially covered by graphene and its bilayer. The line scan profile shows the intensity of transmitted white light along the yellow line. (Inset) Our sample design: A 20-μm-thick metal support structure has several apertures of 20, 30, and 50 μm in diameter with graphene crystallites placed over them. (**B**) Transmittance spectrum of single-layer graphene (open circles). Slightly lower transmittance for λ < 500 nm is probably due to hydrocarbon contamination (*5*). The red line is the transmittance $T = (1 + 0.5\pi\alpha)^{-2}$ expected for two-dimensional Dirac fermions, whereas the green curve takes into account a nonlinearity and triangular warping of graphene's electronic spectrum. The gray area indicates the standard error for our measurements (*5*). (Inset) Transmittance of white light as a function of the number of graphene layers (squares). The dashed lines correspond to an intensity reduction by $\pi\alpha$ with each added layer.

perpendicular to a graphene sheet of a unit area. The incident energy flux W_i is given by $W_i = \frac{c}{4\pi}|\Theta|^2$. Taking into account the momentum conservation $\boldsymbol{k}$ for the initial $|i\rangle$ and final $|f\rangle$ states, only the excitation processes pictured in Figure S5 contribute to the light absorption. The absorbed energy $W_a = \eta\hbar\omega$ is given by the number η of such absorption events per unit time and can be calculated by using Fermi's golden rule as $\eta = (2\pi/\hbar)|M|^2 D$ where M is the matrix element for the interaction between light and Dirac fermions, and D is the density of states at $\varepsilon = E/2 = \hbar\omega/2$ (see Fig. S5). For 2D Dirac fermions, $D(\hbar\omega/2) = \hbar\omega/\pi\hbar^2 v_F^2$ and is a linear function of ε.

The interaction between light and Dirac fermions is generally described by the Hamiltonian

$$\hat{H} = v_F \vec{\sigma}\cdot\vec{p} = v_F \vec{\sigma}\cdot(\hat{p} - \frac{e}{c}\vec{A}) = \hat{H}_0 + \hat{H}_{int}$$

where the first term is the standard Hamiltonian for 2D Dirac quasiparticles in graphene (*S11*) and $\hat{H}_{int} = -v_F \vec{\sigma}\cdot\frac{e}{c}\vec{A} = v_F \vec{\sigma}\cdot\frac{e}{i\omega}\vec{\Theta}$ describes their interaction with electromagnetic field. Here $\vec{A} = \frac{ic}{\omega}\vec{\Theta}$ is the vector potential and $\vec{\sigma}$ the standard Pauli matrices. Averaging over all initial and final states and taking into account the valley degeneracy, our calculations yield

$$|M|^2 = |\langle f| v_F \vec{\sigma}\cdot\frac{e}{i\omega}\vec{\Theta}|i\rangle|^2 = \frac{1}{8} e^2 v_F^2 \frac{|\Theta|^2}{\omega^2}.$$

This results in $W_a = (e^2/4\hbar)|\Theta|^2$ and, consequently, absorption $P = W_a/W_i = \pi e^2/\hbar c = \pi\alpha$, both of which are independent of the material parameter v_F that cancels out in the calculations of W_a. Also note that the dynamic conductivity $G \equiv W_a/|\Theta|^2$ is equal to $e^2/4\hbar$. Because graphene practically does not reflect light ($R \ll 1$ as discussed above), its opacity ($1 - T$) is dominated by the derived expression for P.

In the case of a zero-gap semiconductor with a parabolic spectrum (e.g., bilayer graphene at low ε), the same analysis based on Fermi's golden rule yields $P = 2\pi\alpha$. This shows that the fact that the optical properties of graphene are defined by the fundamental constants is related to its 2D nature and zero energy gap and does not directly involve the chiral properties of Dirac fermions.

On a more general note, graphene's Hamiltonian $\hat{H}$ has the same structure as for relativistic electrons (except for coefficient v_F instead of the speed of light c). The interaction of light with relativistic particles is described by a coupling constant, a.k.a. the fine structure constant. The Fermi velocity is only a prefactor for both Hamiltonians $\hat{H}_0$ and $\hat{H}_{int}$ and, accordingly, one can expect that the coefficient may not change the strength of the interaction, as indeed our calculations show.

Otra obra de alto impacto tecnológico

``Gecko tape´´

Microfabricated adhesive mimicking gecko foot-hair

A. K. GEIM*[1], S. V. DUBONOS[1,2], I. V. GRIGORIEVA[1], K. S. NOVOSELOV[1], A. A. ZHUKOV[2] AND S. YU. SHAPOVAL[2]

[1]Department of Physics & Astronomy, University of Manchester, Manchester M13 9PL, UK
[2]Institute for Microelectronics Technology, 142432 Chernogolovka, Russia
*e-mail: geim@man.ac.uk

Published online: 1 June 2003; doi:10.1038/nmat917

The amazing climbing ability of geckos has attracted the interest of philosophers and scientists alike for centuries[1–3]. However, only in the past few years[2,3] has progress been made in understanding the mechanism behind this ability, which relies on submicrometre keratin hairs covering the soles of geckos. Each hair produces a miniscule force ≈10^{-7} N (due to van der Waals and/or capillary interactions) but millions of hairs acting together create a formidable adhesion of ≈10 N cm^{-2}: sufficient to keep geckos firmly on their feet, even when upside down on a glass ceiling. It is very tempting[3] to create a new type of adhesive by mimicking the gecko mechanism. Here we report on a prototype of such 'gecko tape' made by microfabrication of dense arrays of flexible plastic pillars, the geometry of which is optimized to ensure their collective adhesion. Our approach shows a way to manufacture self-cleaning, re-attachable dry adhesives, although problems related to their durability and mass production are yet to be resolved.

In principle, any submicrometre object—whether it is the tip of an atomic force microscope (AFM), a small piece of dust or a single gecko hair—sticks to a solid surface with an adhesive force in the range 10 to 1,000 nN, depending on the exact geometry and materials involved[2–6]. In the case of hydrophilic materials, it is often an atomic layer of absorbed water (capillary force) that is responsible for the adhesion[4,5]. The capillary force decreases with decreasing a characteristic size R of an object, and can be estimated as $F_c = \sigma R$ where σ is the surface tension of water. On a submicrometre scale, van der Waals interaction is also no longer negligible and can compete with the capillary force. A typical value of van der Waals forces for a submicrometre object is ≈100 nN, and this force becomes dominant in the case of hydrophobic surfaces[2–5]. It is interesting to note that diameters of gecko foot-hair (0.2 to 0.5 μm) fall exactly in the range where the two forces become comparable[3]. This probably indicates that, in the course of evolution, geckos have developed their foot hairs to be of the most appropriate diameter to exploit both the van der Waals and capillary forces, and to climb surfaces of various hydrophilicities.

Based on the understanding of the gecko's climbing mechanism, an AFM tip has been used to produce a set of dimples on a wax surface, which was then used as a mould for making a number of mesoscopic polymer pyramids[3]. With the help of another AFM cantilever with a flat tip, the adhesive force to an individual pyramid was measured. The force

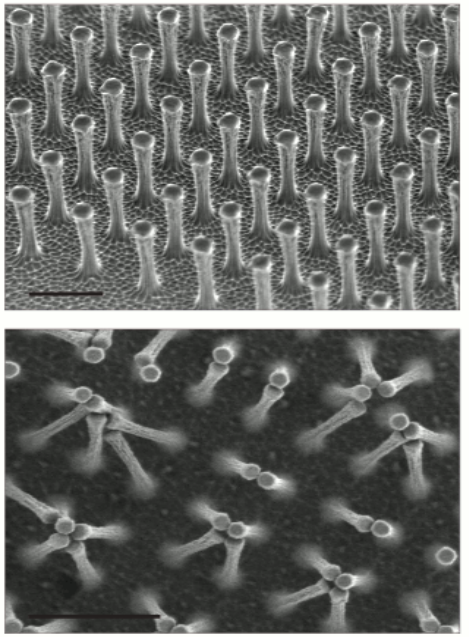

Figure 1 Scanning electron micrographs of microfabricated polyimide hairs. **a**, A small area near the edge of a 1 cm^2 array of polyimide hairs. This array was later used to evaluate macroscopic adhesive properties of the mimetic material. **b**, Bunching is found to be one of the mechanisms responsible for the reduction of adhesive strength of the artificial hair. This micrograph also demonstrates the high flexibility of polyimide pillars. Both scale bars are 2 μm.

Otros premios recibidos

2007 Mott medal del Institute of Physics

2008 EuroPhysics Prize

2009 Körber European Science Award

2009 Carty Award, United States National Academy of Science.

2010 Commander of the Order of the Netherlands Lion.

Premio Ig Nobel

Andre Geim: Premio Ig Nobel en Física 2000

Eur. J. Phys. 18 (1997) 307–313. Printed in the UK

PII: S0143-0807(97)84689-2

Of flying frogs and levitrons

M V Berry† and A K Geim‡

† H H Wills Physics Laboratory, Tyndall Avenue, Bristol BS8 1TL, UK
‡ High Field Magnet Laboratory, Department of Physics, University of Nijmegen, Toernooiveld, 6525 ED Nijmegen, The Netherlands

Received 4 June 1997

Abstract. Diamagnetic objects are repelled by magnetic fields. If the fields are strong enough, this repulsion can balance gravity, and objects levitated in this way can be held in stable equilibrium, apparently violating Earnshaw's theorem. In fact Earnshaw's theorem does not apply to induced magnetism, and it is possible for the total energy (gravitational + magnetic) to possess a minimum. General stability conditions are derived, and it is shown that stable zones always exist on the axis of a field with rotational symmetry, and include the inflection point of the magnitude of the field. For the field inside a solenoid, the zone is calculated in detail; if the solenoid is long, the zone is centred on the top end, and its vertical extent is about half the radius of the solenoid. The theory explains recent experiments by Geim *et al*, in which a variety of objects (one of which was a living frog) was levitated in a field of about 16 T. Similar ideas explain the stability of a spinning magnet (Levitron™) above a magnetized base plate. Stable levitation of paramagnets is impossible.

Samenvatting. Magnetische velden stoten diamagnetische voorwerpen af. Zulke velden kunnen zo sterk zijn dat zij de zwaartekracht opheffen. Het is op deze wijze mogelijk zulke voorwerpen te laten zweven. Dit vormt een stabiel evenwicht, wat in tegenspraak schijnt te zijn met Earnshaw's Theorema. Echter Earnshaw's Theorema is niet langer geldig als het magnetisme veld geinduceerd is. De totale energie (bevattende bijdragen van het magnetisme en de zwaartekracht) kan toch een lokaal minimum vertonen. Algemene criteria voor zo'n minimum zullen worden opgesteld. Verder zal worden aangetoond dat voor een cilindrisch symmetrisch veld, langs zijn symmetrie as altijd een zone gevonden kan worden waarin een stabiel evenwicht bestaat. Voor het veld binnen een solenoïde zal deze zone in detail bepaald worden. Als deze spoel voldoende land is bevindt deze zone zich aan het uiteinde van de spoel. De lengte van deze zone langs de symmetrie as van het veld is ongeveer de helft van de straal van de spoel. Deze theorie geeft een goede verklaring voor de experimenten van Geim *et al*. In deze experimenten werden een grote verscheidenheid aan verschillende voorwerpen (waaronder een levende kikker)

Premio Ig Nobel en Física 2000

Dato humorístico

ELSEVIER

Physica B 294–295 (2001) 736–739

PHYSICA B

www.elsevier.com/locate/physb

Detection of earth rotation with a diamagnetically levitating gyroscope

A.K. Geim*, H.A.M.S. ter Tisha

High Field Magnet Laboratory, University of Nijmegen, Toernooiveld 1, 6525 ED Nijmegen, The Netherlands

Abstract

Strong magnetic fields allow levitation of apparently nonmagnetic substances due to their weak but not negligible diamagnetic response of about 10^{-5}. Importantly, the diamagnetic force compensates gravity on the level of individual atoms and molecules and, therefore, can be used to mimic a continuous zero-gravity environment that, otherwise, is only achievable on board of a space station. Here we employ this earth-bound low gravity to demonstrate a simple mechanical gyroscope with sensitivity already comparable to that achieved by quantum and military gyroscopes. Our gyroscope can serve as a "shooting range" for the development of precision orbiting gyroscopes that have been a subject of intensive discussions regarding possible tests of general relativity.

Keywords: Levitation; Gyroscope; Diamagnetism

1. Introduction

Although Foucault's pendulum allowed accurate measurements of the earth rotation more than a century ago, detection of very slow absolute rotations continues to present a formidable scientific

and it is practically impossible to suppress such drifts to a level below $10^{-3}\,\Omega_E$. A new generation of quantum gyroscopes based on the interference of light or matter promise to rival the mechanical gyroscopes [1] and have recently demonstrated the absolute accuracy between 0.1% and 1% of Ω_E

Agradecimiento

Gilles Montambaux, Curso de Grafeno, Escuela Giambiagi 2010, www.df.uba.ar